Shape Coexistence in ^{78}Ni as the Portal to the Fifth Island of Inversion

F. Nowacki,[1,2] A. Poves,[3] E. Caurier,[1,2] and B. Bounthong[1,2]
[1]Université de Strasbourg, IPHC, 23 rue du Loess 67037 Strasbourg, France
[2]CNRS, UMR7178, 67037 Strasbourg, France
[3]Departamento de Física Teórica e IFT-UAM/CSIC, Universidad Autónoma de Madrid, E-28049 Madrid, Spain and Institute for Advanced Study, Université de Strasbourg, France

(Received 30 May 2016; revised manuscript received 14 July 2016; published 27 December 2016)

Large-scale shell-model calculations predict that the region of deformation which comprises the heaviest chromium and iron isotopes at and beyond $N = 40$ will merge with a new one at $N = 50$ in an astonishing parallel to the $N = 20$ and $N = 28$ case in the neon and magnesium isotopes. We propose a valence space including the full pf shell for the protons and the full sdg shell for the neutrons, which represents a comeback of the the harmonic oscillator shells in the very neutron- rich regime. The onset of deformation is understood in the framework of the algebraic SU(3)-like structures linked to quadrupole dominance. Our calculations preserve the doubly magic nature of the ground state of ^{78}Ni, which, however, exhibits a well-deformed prolate band at low excitation energy, providing a striking example of shape coexistence far from stability. This new IOI adds to the four well-documented ones at $N = 8$, 20, 28, and 40.

DOI: 10.1103/PhysRevLett.117.272501

Introduction.—The limits of the nuclear stability and the origin of the chemical elements in the Universe are burning issues in nuclear physics. These fundamental questions pose a major challenge to our theoretical understanding of nuclei, in particular towards the neutron drip line, given the important role played by the structure of neutron-rich nuclei in numerous astrophysical processes [1]. A peculiar manifestation of the nuclear dynamics, absent in most interacting fermionic systems, is the phenomenon of shape coexistence, i.e., the appearance of quantum states of very different shapes very close in energy, typically much smaller than what could be anticipated in a mean-field description [2]. This is a major consequence of the dominant role of the correlations in the nucleus. The experimental exploration of regions of very neutron-rich nuclei has recently unveiled the presence of a rich variety of shape coexistence scenarios in this sector of the nuclear chart. They are particularly frequent at the edge of the so-called islands of inversion (IOIs), which appear close to semimagic or even doubly magic nuclei. The IOIs are formed when a group of nuclei, expected to be spherical in their ground states, becomes deformed, precisely because the strong nuclear quadrupole-quadrupole interaction produces a shape transition in which highly correlated many-particles-many-holes configurations dubbed "intruders" turn out to be more bound than the spherical ones. These intruder deformed bands often appear at low excitation energy in the magic nuclei close to the IOIs; hence, shape coexistence acts in fact as a portal to the IOIs. An intense experimental program [3–12] has recently explored the details of the shape coexistence in ^{68}Ni and the existence of a new IOI surrounding ^{64}Cr. Large-scale shell-model calculations predicted first, and later explained in detail, this behavior [13,14], with particular emphasis in the strong similarity of the mechanisms driving the onset of deformation and the collapse of the shell closures at $N = 20$ and $N = 40$. Another recent experimental and theoretical finding is the merging of the IOIs at $N = 20$ and $N = 28$ [15,16]. In view of these precedents, we wondered if a new IOI might exist at $N = 50$ and if an equivalent phenomenon of IOIs merging occurs for $N = 40$ and $N = 50$. These questions prompted this study, whose results support fully both conjectures. In the meantime, there have been new experimental measures on the chromium and iron isotopes up to $N = 42$ and $N = 46$, respectively, which seem to support it as well [17], and interesting theoretical and experimental explorations of the physics close to ^{78}Ni [18–20], which have helped us a lot in the present investigation. The trends in the evolution of the spherical mean field, which favor the appearance of the IOIs, have been discussed in Ref. [21].

The valence space.—Why should intruder configurations produce shape coexistence in ^{78}Ni and deformed ground states in ^{76}Fe and ^{74}Cr? Because the outcome depends on the interplay of the spherical mean field and the quadrupole-quadrupole correlations. Therefore, we must ensure that the chosen valence space can incorporate the latter properly. Because of the similarity between the $N = 20$–28 and the $N = 40$–50 regions, we chose to define an interaction covering the pf-sdg valence space that parallels what we did successfully for the sd-pf case [16,22]. It is well known that quadrupole collectivity is maximized when the orbits close to the Fermi level permit the realization of two variants of Elliott's SU(3) [23–25]; pseudo-SU(3), which applies when all the orbits of a major oscillator shell except the one with the largest $\mathbf{j}$ are quasidegenerated, and quasi-SU(3) when the orbit with the largest $\mathbf{j}$ and its $\Delta j = 2$ $\Delta l = 2$ partners are quasidegenerated. For the protons,

the natural space beyond $Z = 20$ and up to $Z = 32$–34 is indeed the full pf shell, which will bring in quadrupole collectivity of quasi- or pseudo-SU(3) type, depending on the number of protons and the value of the $Z = 28$ gap. In the neutron side, as we add neutrons in excess of $N = 40$, the role of the neutron pf shell orbits is slowly transferred to the companions of the $0g_{9/2}$ orbit in the sdg major oscillator shell. Unfortunately, size prevents us from following the transition from $N = 40$ to $N = 50$, keeping both sets of neutron orbits in our valence space, but we expect a smooth transit from one space to another. The borderline between the space of Ref. [17] and the present one can be loosely located at $N = 46$. Just at the transition point, it could be advisable to include the $1p_{1/2}$ neutron orbit as well. In the $N = 40$ valence space, the neutron collectivity is provided by the pseudo-SU(3) coherence of the holes below $N = 40$ and the quasi-SU(3) coherence of the particles above it, and the mean-field regulator is the $N = 40$ gap. Close to $N = 50$, the buildup of collectivity is different. Neutrons above $N = 50$ can develop pseudo-SU(3) coherence, whereas neutron holes in the $0g_{9/2}$ neutron orbit help with their single-shell-prolate-quadrupole moment. The mean-field regulator is now the $N = 50$ gap. In brief, the valence space proposed in this article comprises the $p = 3$ harmonic oscillator [HO, $E(p) = \hbar\omega(p + 1/2)$] shell ($pf$) for the protons and the $p = 4$ HO shell (sdg) for the neutrons. Thus, compared to that of Ref. [13], the new valence space corresponds to closing the pf shell and includes the missing sdg shell orbits for the neutrons, using an inert core of ^{60}Ca.

The effective interaction.—Our starting effective interaction matrix elements are based on the free nucleon-nucleon interaction of Ref. [26], regularized and renormalized with the G-matrix techniques of Ref. [27]. We modify their monopole part in order to reproduce the experimental evolution of the regulating gaps in the model space. Following the previous study of ^{78}Ni in [18], we have left unchanged most of the monopoles of the LNPS interaction and, to fix the remaining ones, we have adjusted the neutron ESPEs to reproduce the experimental binding energies of the nickel isotopes (S_n for $A = 69$ and S_{2n} for $A = 68$–72), the binding energies of the zirconium isotopes for $A = 90$–98, and the neutron gaps in the $N = 50$ isotones. The size of the $Z = 28$ proton gap is controlled by the $B(E2)$s from the first excited 2^+ states to the 0^+ ground states of the zinc and germanium isotopes around $N = 50$. We adopt for ^{79}Cu the single particle spectrum of the JUN45 interaction [28]. Finally, the ^{79}Ni single-particle spectrum and the cross-shell pf-sdg proton-neutron monopoles are constrained by the $N = 49$ and $N = 51$ available data. In particular to reproduce the relative location of the $9/2^+$, $5/2^+$, and $1/2^+$ states in the $N = 49$ isotones and their evolution from $Z = 30$ [20] to $Z = 32$–40 [29]. The final values of the effective single particle energies are gathered in Fig. 1. We name the resulting interaction PFSDG-U. The dimensions of the matrices to be diagonalized are at the edge of present computer capabilities for solving the problem exactly, in several cases reaching 2×10^{10} Slater determinants.

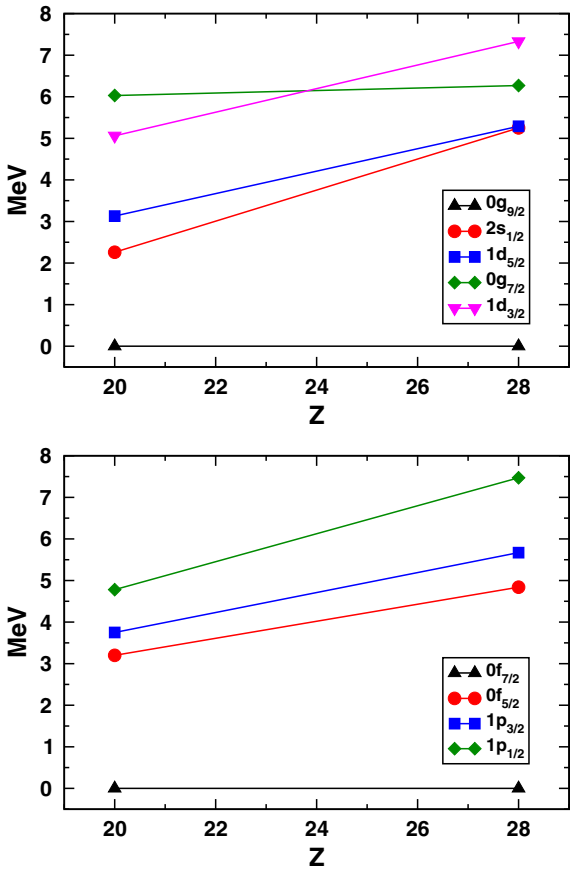

FIG. 1. Effective single neutron energies at $N = 50$ (upper panel) and effective single proton energies at $N = 50$ (lower panel).

Projected energy surfaces.—To unveil the presence of intrinsic structures underlying our shell-model configuration-interaction (SM CI) results in the laboratory frame, we have performed constrained Hartree-Fock (CHF) calculations in the pf-sdg valence space using the PFSDG-U interaction. We solve the Hartree-Fock equations constrained by the quadrupole deformation parameters β and γ—which break rotational invariance and thus produce deformed shapes—to obtain the energy as a function of these parameters. The results are displayed as contour plots in the (mass) β-γ plane (also known as projected energy surfaces PES) in Fig. 2. It is seen that at the mean-field level, ^{78}Ni is an spherical doubly magic nucleus in its ground state with local deformed oblate and prolate minima. ^{76}Fe has instead three minima: spherical, prolate, and oblate, the latter two connected by the γ degree of freedom. In the case of ^{74}Cr, the landscape is fully dominated by the prolate solution. These deformed structures have typically $\beta \sim 0.3$.

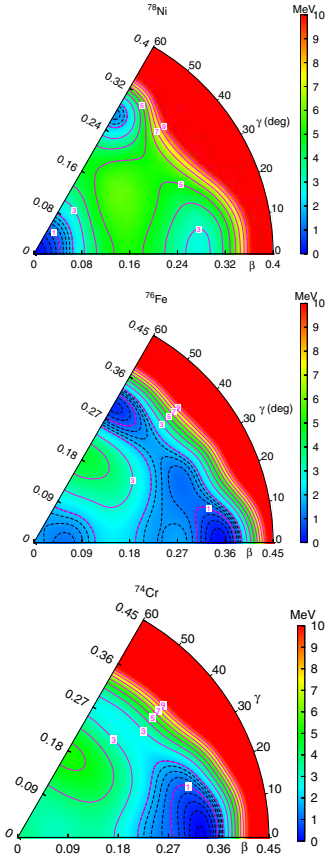

FIG. 2. Projected Energy Surfaces for ^{78}Ni, ^{76}Fe, and ^{74}Cr with the interaction PFSDG-U.

Spectroscopic results.—Let's move now to the predictions of the full-fledged diagonalizations using the interaction PFSDG-U, starting with the results at a fixed number of neutron excitations across the $N = 50$ closure. For this calculation, we do not impose any truncation in the proton space. The structure of the 2p-2h and 4p-4h bands are very similar for all the isotopes (except for ^{70}Ca) and correspond to well-deformed rotors with a nearly perfect $J(J+1)$ spacing, and $B(E2)$ is consistent with deformation parameters very close to the ones obtained in the SU(3) limit (we use standard effective charges $q_\pi = 1.31$ and $q_\nu = 0.46$). For the 2p-2h yrast band of ^{74}Cr, we have $E(2^+) = 0.27$ MeV and $B(E2)(2_1^+ \to 0_2^+) = 360\ e^2\,\mathrm{fm}^4$, whereas for the 4p-4h one, we get $E(2^+) = 0.17$ MeV and $B(E2)(2_1^+ \to 0_2^+) = 555\ e^2\,\mathrm{fm}^4$. We have estimated the correlation energies of the 2p-2h and 4p-4h neutron configurations, diagonalizing a properly normalized quadrupole interaction in the *sdg* space for the neutrons and the quasi-*pf* doublet for the protons. The results are displayed in Table I. It is seen that both for the 2p-2h and 4p-4h cases, the largest correlation energies correspond to ^{74}Cr and ^{76}Fe, followed by those of ^{78}Ni and ^{72}Ti. Notice that removing protons from ^{78}Ni, the intruder configurations will benefit from the gain in correlation energy *and* from the reduction of the $N = 50$ neutron gap; therefore, we may expect an abrupt shape change producing an IOI.

TABLE I. Quadrupole correlation energies of the neutron intruder configurations, relative to the $N = 50$ closure (in MeV).

	^{78}Ni	^{76}Fe	^{74}Cr	^{72}Ti	^{70}Ca
2p-2h	5.3	6.5	7.0	5.3	2.2
4p-4h	9.3	10.9	11.3	9.1	4.8

For the full diagonalizations, we use a truncation scheme in terms of the sum of the number of neutron excitations across $N = 50$ and proton excitations across $Z = 28$ (t). We perform full-space calculations for Ca, Ti, and Cr and we are limited to $t = 8$ for Ni and Fe, but the calculations seem to be converged. For ^{78}Ni (see Fig. 3), we predict a doubly magic ground state at 65%, with a first 2^+ excited state at 2.88 MeV, which belongs to the (prolate) deformed band based in the intruder 0^+, which appears at an excitation energy of 2.65 MeV, and a second 2^+ of 1p-1h nature at 3.15 MeV, connected to the ground state with $B(E2) = 110\ e^2\,\mathrm{fm}^4$. We have plotted as well the yrast 4^+, which belongs to the deformed band, its 6^+ member, and several states of particle-hole nature. The $B(E2)(2_1^+ \to 0_2^+)$ goes up to 516 $e^2\,\mathrm{fm}^4$. The location of the intruder band depends of the competition of the monopole losses, whose linear part is given by the neutron ESPEs and the correlation gains (see Table I). In ^{78}Ni, the balance favors the closed shell, with the intruder 2p-2h (neutron) band below 3 MeV. Removing two protons in ^{76}Fe, the $N = 50$ gap is reduced and the correlation energy increased. This produces an abrupt lowering of the intruder configurations whose bandheads become nearly degenerated with the 0p-0h $N = 50$ closure. Hence, the ground state of ^{76}Fe turns out to be a very complicated mixture of np-nh configurations, including 21% of 0p-0h and 33% of neutron 2p-2h. The yrast 2^+ appears at 0.43 MeV and it is rather of 2p-2h plus 4p-4h nature. This mismatch produces a certain quenching of the $B(E2)$ relative to the spectroscopic quadrupole moment of the 2^+ as seen in Table II. Most interestingly, the first excited state is another 0^+ at 0.36 MeV, which is also of very mixed nature, although

TABLE II. Some $E2$ properties of the $N = 50$ isotones. Energies in MeV, $B(E2)$'s in $e^2\,\mathrm{fm}^4$, Q's in $e\,\mathrm{fm}^2$.

	ΔE			$B(E2)\downarrow$			Q_s		
	2^+	4^+	6^+	2^+	4^+	6^+	2^+	4^+	6^+
^{78}Ni	2.88	3.45	4.14	32	783	1021	−39	−65	−75
^{76}Fe	0.43	1.05	1.90	314	707	969	−45	−57	−63
^{74}Cr	0.24	0.72	1.38	630	911	1004	−51	−66	−74
^{72}Ti	0.41	1.02	1.78	321	506	580	−34	−45	−53
^{70}Ca	0.91	1.80	2.56	119	194	5	−3	+8	+8

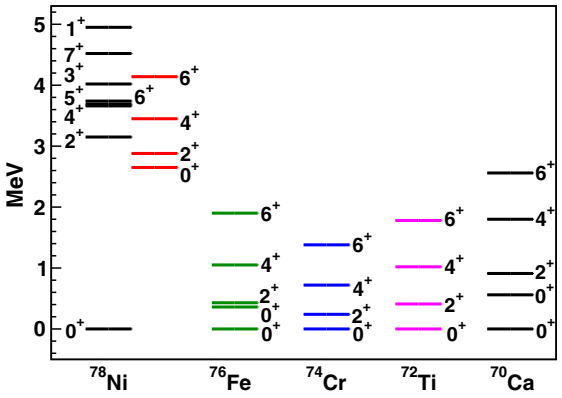

FIG. 3. Theoretical spectra of the $N = 50$ isotones with the PFSDG-U interaction. In red the deformed intruder band of ^{78}Ni.

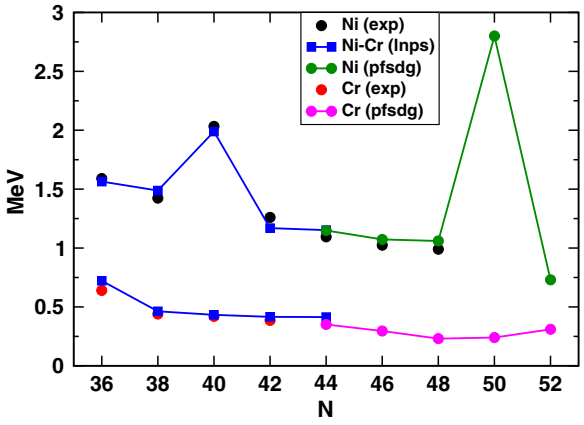

FIG. 4. 2^+ energy systematics in the nickel and chromium isotopic chains. Experimental data compared with calculations using the LNPS [13] and PFSDG-U interactions.

now the 0p-0h components amount to 33%. The distortion of the spectrum is due to the mixing of the spherical and the deformed 0^+'s. Thus, the doublet of 0^+ states in ^{76}Fe signals the rapid transition from the doubly magic ground state of ^{78}Ni to the fully rotational case of ^{74}Cr, where the collective behavior is well established, and the neutron 4p-4h intruder becomes dominant in the yrast band, with a 2^+ at 0.27 MeV and $E(4^+)/E(2^+) = 3$ (see Fig. 3). Collectivity persists to a lesser extent in ^{72}Ti, whose 2^+ is at 0.41 MeV. There is no experimental information for these nuclei yet. Table II shows the calculated $B(E2)$ values and spectroscopic quadrupole moments, which correspond, in the well-deformed case of ^{74}Cr, to $\beta_{\text{mass}} \sim 0.32$ and $\beta_{\text{charge}} \sim 0.35$ in very nice agreement with the results of the CHF PES. In Table III, we display the occupation numbers of the neutron and proton orbits above the $N = 50$, $Z = 28$ doubly magic closure. It is seen that in the neutron side, they evolve from 2.7 neutrons excited in ^{78}Ni to a maximum of 4.9 neutrons in ^{74}Cr, and down to 3.3 neutrons in ^{70}Ca. Importantly, we verify that in all the cases, all the excited orbits have non-negligible occupations, as expected in a pseudo-SU(3) regime, which, however, is only fully dominant in ^{74}Cr. In the proton sector, the $p_{3/2}$ orbit is preferentially populated, as should happen in the quasi-SU(3) limit, except in ^{78}Ni, where the proton collectivity is rather of pseudo-SU(3) type. ^{70}Ca is the most neutron-rich nuclei in our palette and the one for which our predictions are less dependable because of the far-off extrapolation of the neutron ESPEs. It has a curious structure, more vibrational than superfluid, with its ground state wave function evenly split (24/24/21/16)% between the (0/2/4/6)p-h configurations, and a first excited 0^+ state at about 500 keV of doubly magic, $N = 50$, $Z = 20$, character.

TABLE III. Average number of p-h excitations and occupancies of the neutron and proton orbits above $N = 50$ and $Z = 28$ for several intruder states.

	$n^{\nu}_{\text{p-h}}$	$n^{\pi}_{\text{p-h}}$	$d^{\nu}_{5/2}$	$s^{\nu}_{1/2}$	$g^{\nu}_{7/2}$	$d^{\nu}_{3/2}$	$p^{\pi}_{3/2}$	$f^{\pi}_{5/2}$	$p^{\pi}_{1/2}$
^{78}Ni 0^+_2	2.7	2.3	1.1	0.8	0.4	0.4	0.9	1.0	0.4
^{76}Fe 2^+_1	3.0	1.4	1.2	0.8	0.6	0.4	0.8	0.4	0.2
^{74}Cr 0^+_1	4.9	1.6	1.8	1.1	1.2	0.8	1.1	0.3	0.2
^{72}Ti 0^+_1	4.8	0.9	2.2	0.7	0.6	1.3	0.7	0.1	0.1
^{70}Ca 0^+_1	3.5	0.0	1.9	0.3	0.2	1.1	0.0	0.0	0.0

Finally, we gather in Fig. 4, the evolution of the 2^+ excitation energies for the nickel and chromium chains. The present calculations are complemented towards $N = 40$, with the results obtained using the LNPS interaction and valence space [13]. It is seen that the magic peaks in the nickels, at $N = 40$ and $N = 50$, disappear completely in the chromiums: the fingerprint of the onset of deformation and of the entrance in the IOIs. The same is indeed true for the iron chain. The agreement of the SM CI description with experiment may soon extend to full chains of isotopes from the proton to the neutron drip lines, for instance, from ^{48}Ni and ^{44}Cr ($N = 20$) in the pf shell with the KB3G interaction, to ^{80}Ni and ^{76}Cr ($N = 52$) using PFSDG-U.

In conclusion, it looks as if nature would like to replicate the $N = 40$ physics at $N = 50$. Shape coexistence in doubly magic ^{78}Ni turns out to be the portal to a new IOI at $N = 50$, which merges with the well established one at $N = 40$ for the isotopes with $Z \leq 26$. With this new addition, the archipelago of IOIs in the neutron rich shores of the nuclear chart counts now five members: $N = 8$, 20, 28, 40, and 50.

This work is partly supported by MINECO (Spain) Grant No. FPA2014-57196 and Programme "Centros de Excelencia Severo Ochoa" SEV-2012-0249, and by an USIAS Fellowship of the Université de Strasbourg.

Note added.—A paper describing the heaviest nickel isotopes with "*ab initio*" methods has appeared in [30]

very recently. Whereas both calculations agree in many aspects, they differ in the absence in the latter of the intruder, deformed, np-nh excited band, coexisting with the particle-hole states built upon the doubly magic ground state of ^{78}Ni.

[1] R. N. Wolf *et al.*, Phys. Rev. Lett. **110**, 041101 (2013).
[2] K. Heyde and J. Wood, Rev. Mod. Phys. **83**, 1467 (2011).
[3] O. Sorlin *et al.*, Phys. Rev. Lett. **88**, 092501 (2002).
[4] M. Hannawald *et al.* Phys. Rev. Lett. **82**, 1391 (1999).
[5] W. Rother *et al.*, Phys. Rev. Lett. **106**, 022502 (2011).
[6] J. Ljungvall *et al.*, Phys. Rev. C **81**, 061301 (2010).
[7] A. Gade *et al.*, Phys. Rev. C **81**, 051304 (2010).
[8] A. Dijon *et al.* Phys. Rev. C **85**, 031301 (2012).
[9] F. Recchia *et al.* Phys. Rev. C **88**, 041302(R) (2013).
[10] S. Suchyta *et al.* Phys. Rev. C **89**, 021301(R) (2014).
[11] T. Baugher *et al.* Phys. Rev. C **86**, 011305(R) (2012).
[12] H. L. Crawford *et al.* Phys. Rev. Lett. **110**, 242701 (2013).
[13] S. M. Lenzi, F. Nowacki, A. Poves, and K. Sieja, Phys. Rev. C **82**, 054301 (2010).
[14] Y. Tsunoda, T. Otsuka, N. Shimizu, M. Honma, and Y. Utsuno, Phys. Rev. C **89**, 031301(R) (2014).
[15] P. Doornenbal *et al.*, Phys. Rev. Lett. **111**, 212502 (2013).
[16] E. Caurier, F. Nowacki, and A. Poves, Phys. Rev. C **90**, 014302 (2014).
[17] C. Santamaria *et al.*, Phys. Rev. Lett. **115**, 192501 (2015).
[18] K. Sieja and F. Nowacki, Phys. Rev. C **81**, 061303 (2010); **85**, 051301 (2012).
[19] A. Gottardo *et al.*, Phys. Rev. Lett. **116**, 182501 (2016).
[20] X. F. Yang *et al.*, Phys. Rev. Lett. **116**, 182502 (2016).
[21] O. Sorlin, EPJ Web Conf. **66**, 01016 (2014).
[22] J. Retamosa, E. Caurier, F. Nowacki, and A. Poves, Phys. Rev. C **55**, 1266 (1997).
[23] A. P. Zuker, A. Poves, F. Nowacki, and S. M. Lenzi, Phys. Rev. C **92**, 024320 (2015).
[24] A. Arima, M. Harvey, and K. Shimizu, Phys. Lett. B **30**, 517 (1969).
[25] K. Hecht and A. Adler, Nucl. Phys. **A137**, 129 (1969).
[26] R. Machleidt, Phys. Rev. C **63**, 024001 (2001).
[27] M. Hjorth-Jensen, T. T. S. Kuo, and E. Osnes, Phys. Rep. **261**, 125 (1995).
[28] M. Honma, T. Otsuka, T. Mizusaki, and M. Hjorth-Jensen, Phys. Rev. C **80**, 064323 (2009).
[29] National Nuclear Data Center, http://www.nndc.bnl.gov/.
[30] G. Hagen, G. R. Jansen, and T. Papenbrock, Phys. Rev. Lett. **117**, 172501 (2016).